Journal of the Korean Ceramic Society
Vol. 53, No. 4, pp. 463~467, 2016.

http://dx.doi.org/10.4191/kcers.2016.53.4.463

Synthesis and Luminescence of $Lu_3(Al,Si)_5(O,N)_{12}:Ce^{3+}$ Phosphors

Wonsik Ahn and Young Jin Kim†

Department of Advanced Materials Engineering, Kyonggi University, Suwon 16227, Korea

(Received April 22, 2016; Revised May 19, 2016; Accepted May 19, 2016)

ABSTRACT

Si^{4+}–N^{3-} was incorporated into Ce^{3+}-doped lutetium aluminum garnet ($Lu_{2.965}Ce_{0.035}Al_5O_{12}$, LuAG:$Ce^{3+}$) lattices, resulting in the formation of $Lu_{2.965}Ce_{0.035}Al_{5-x}Si_xO_{12-x}N_x$ [(Lu,Ce)AG:*x*SN]. For x = 0–0.25, the synthesized powders consisted of the LuAG single phase, and the lattice constant decreased owing to the smaller Si^{4+} ions. However, for x > 0.25, a small amount of unknown impurity phases was observed, and the lattice constant increased. Under 450 nm excitation, the PL spectrum of LuAG:Ce^{3+} exhibited the green band, peaking at 505 nm. The incorporation of Si^{4+}–N^{3-} into the Al^{3+}–O^{2-} sites of LuAG:Ce^{3+} led to a red-shift of the emission peak wavelength from 505 to 570 nm with increasing x. Corresponding CIE chromaticity coordinates varied from the green to yellow regions. These behaviors were discussed based on the modification of the $5d^1$ split levels and crystal field surroundings of Ce^{3+}, which arose from the Ce–(O,N)8 bonds.

Key words : Lutetium aluminum garnet, Phosphors, Luminescence, Nitridation

1. Introduction

Solid-state lightings (SSLs) have attracted great attention because of their high luminous efficiency, long lifetime, energy-saving potential, etc. One of the prevailing SSL technologies is a phosphor-conversion white light-emitting diode (pc-WLED), which uses a phosphor blend to convert blue or near-ultraviolet light emitted from LED chips into white light. The most popular phosphor materials are nitrides, silicates, aluminates, and phosphates.[1-5)]

In addition, Ce^{3+}-doped $R_3Al_5O_{12}$ garnet systems have been recognized as effective phosphors for use in pc-LEDs combined with blue chips. For example, yttrium aluminum garnet ($Y_3Al_5O_{12}:Ce^{3+}$, YAG:Ce^{3+})[6-13)] and terbium ($Tb_3Al_5O_{12}:Ce^{3+}$, TAG:Ce^{3+})[14)] are commercially used as yellow phosphors. Recently, Ce^{3+}-doped lutetium aluminum garnet ($Lu_3Al_5O_{12}:Ce^{3+}$, LuAG:Ce^{3+}) was reported to have a value of thermal quenching lower than that of YAG:Ce^{3+}; it is also commercially used as a green phosphor alternative to Eu^{2+}-doped β-sialon for high-power pc-WLEDs.[9,15-20)]

LuAG has 160 atoms in a cubic cell (space group: $Ia\bar{3}d$). The Lu and O atoms occupy 24 and 96 sites, respectively, and each Lu atom is coordinated by eight oxygen atoms in a distorted cube. Al atoms occupy two non-equivalent sites, 16 octahedral and 24 tetrahedral.[21)] The photoluminescence excitation (PLE) spectra of the LuAG:Ce^{3+} powders consist of strong (~ 450 nm) and weak (~ 345 nm) peaks, which are assigned to the electrons excited from the ground state (4f) doublet to the $5d^1$ state of the Ce^{3+} ions.[8,19,22)] Corresponding photoluminescence (PL) spectra show single emission bands in the green region, which are the result of the two overlapping subbands assigned to the $^2D \rightarrow {}^2F_{5/2}$, $^2F_{7/2}$ transitions of the Ce^{3+} ions.[15-20)]

For the YAG:Ce^{3+} powders, the effects of the incorporation of Si^{4+}–N^{3-} on the luminescence have been reported in many earlier studies,[9-13)] whereas there are only a few works in the literature that consider LuAG:Ce^{3+}.[9,16)] Even though the phase formation and the PL (PLE) spectra of LuAG:Ce^{3+} doped with Si^{4+}–N^{3-} has been the subject of earlier studies, those studies are still lacking in certain aspects: there is very little information on the phase formation for large amounts of Si^{4+}–N^{3-} or investigation into the PL (PLE) spectra assigned to Ce–(O,N)8 bonds. In this work, we prepared LuAG:Ce^{3+} powders and investigated the effects of Si^{4+}–N^{3-} incorporation on the phase formation and the luminescence.

2. Experimental Procedure

$Lu_{2.965}Ce_{0.035}Al_{5-x}Si_xO_{12-x}N_x$ [(Lu,Ce)AG:*x*SN] powders were prepared by a solid-state reaction process using Lu_2O_3 (99.99%, Solvay), Al_2O_3 (99.99%, High Purity Chemicals), α-Si_3N_4 (Ube Industry, Ltd., E10, 99.9%), and CeO_2 (99.99%, Grand Chemical & Materials) as starting materials. 2 wt% AlF_3 (95%, Junsei) flux was added to the starting mixtures, and the relative amounts of AlF_3 and Al_2O_3 were calculated to maintain a stoichiometric Al content. The starting mixtures were ball-milled for 24 h and synthesized at 1700°C for 7 h under a hydrogen (5% H_2 + 95% N_2) atmosphere.

The crystal structure was determined using an X-ray diffractometer (XRD, PANalytical, X'Pert^3 Powder) with $Cu_{K\alpha}$ radiation (λ = 1.5406 Å). Rietveld refinement was performed

†Corresponding author : Young Jin Kim
E-mail : yjkim@kyonggi.ac.kr
Tel : +82-31-249-9766 Fax : +82-31-244-6300

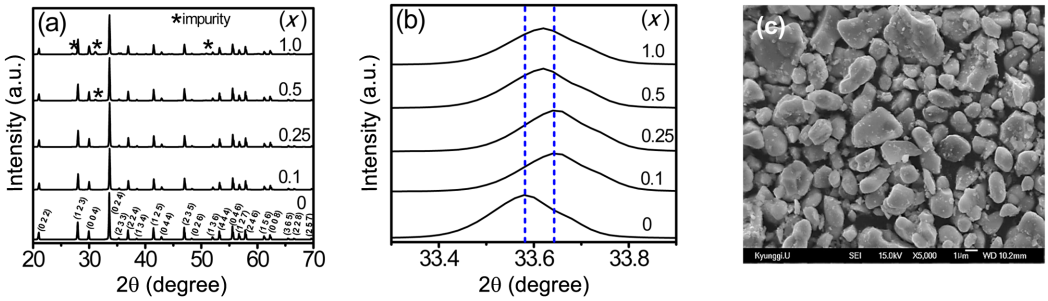

Fig. 1. (a) XRD patterns, (b) enlarged XRD patterns of the (Lu,Ce)AG:*x*SN powders (x = 0, 0.1, 0.25, 0.5, and 1.0), and (c) SEM micrograph for x = 0.25.

using X'Pert HighScore Plus (Ver. 4.1). The nitrogen and oxygen contents of the powders were measured using a nitrogen/oxygen analyzer (HORIBA EMGA-920). The PL spectra were measured using a PL system (PSI, Darsa-5000) with a 500 W xenon lamp as an excitation light source.

3. Results and Discussion

The XRD patterns of the (Lu,Ce)AG:*x*SN (x = 0, 0.1, 0.25, 0.5, and 1.0) powders are shown in Fig. 1(a). For x = 0-0.25, the patterns correspond to those of ICSD #98-002-3846, indicating that Ce^{3+}, Si^{4+}, and N^{3-} ions were fully incorporated into the LuAG lattices. It was most probable that the Si^{4+} (r = 0.26 Å for CN = 4, r = 0.4 Å for CN = 6) and N^{3-} ions (r = 1.46 Å) were substituted for the Al^{3+} (r = 0.39 Å for CN = 4, r = 0.535 Å for CN = 6) and O^{2-} ions (r = 1.38 Å), respectively. As a result, positive $Si_{Al}^{\bullet}$ and negative $N_O^{'}$ defects were created simultaneously and compensated for each other to maintain the charge neutrality. As described above, the Al^{3+} ions are located in the centers of tetrahedra and octahedra, respectively, but the site occupancy factor of the Si^{4+} ions at the Al^{3+} sites is unclear at this stage. On the other hand, further increase to x = 0.5 led to the formation of an impurity phase (marked with *) owing to the solubility limit for Si^{4+}–N^{3-} in LuAG:Ce^{3+}, and its content slightly increased for x = 0.5–1.0. Wang *et al.* also reported similar results for $Y_3Al_{5-x}Si_xO_{12-x}N_x$:$Ce^{3+}$, in which an impurity phase was produced for $x > 0.39$.[11] Liu *et al.*[16] demonstrated that Si^{4+}–N^{3-} could be fully dissolved into the LuAG:Ce^{3+} lattices up to x = 0.27; this finding is nearly consistent with our results. The nitrogen content in the (Lu,Ce)AG:*x*SN powders was measured using an oxygen and nitrogen analyzer. We were able to obtain the nitrogen content [N (%) = 0.884] only for x = 0.1, but not for the other samples. It can be inferred from these findings that the nitrogen content in the powders was too small to be exactly measured. Nevertheless, we were able to confirm that nitrogen ions were incorporated into the LuAG lattices, because the effects of nitrogen atoms on the PL spectra were evident (this will be explained during the discussion of the PL and PLE spectra). It is highly probable that the solubility limit for Si^{4+}–N^{3-} in LuAG:Ce^{3+} is closely correlated with preparation conditions

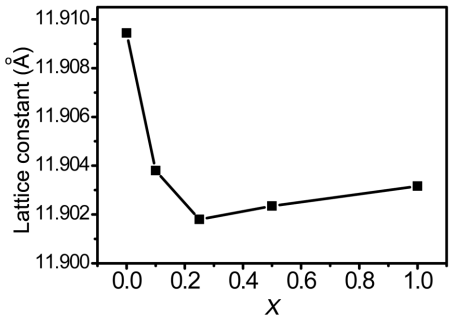

Fig. 2. Lattice constant of the (Lu,Ce)AG:*x*SN powders as a function of x.

such as firing temperatures, flux, Ce^{3+} concentration, etc.[9] The difference in ionic size between Si^{4+} and Al^{3+} (δr = 0.13 and 0.135 Å for CN = 4 and 6, respectively) was larger than that between N^{3-} and O^{2-} (δr = 0.08 Å), leading to a shrinkage of the unit cell of LuAG. In addition, the Si^{4+}–N^{3-} bonds (1.685–1.76 Å in Si_3N_4) are shorter than the Al^{3+}–O^{2-} bonds (1.761 Å in LuAG), which resulted in lattice shrinkage as well.[9,11,12] Accordingly, upon increasing x to 0.25, the main peak moves towards higher diffraction angles (Fig. 1(b)), and the lattice constant gradually decreases, as shown in Fig. 2. However, for x = 0.5–1.0, the XRD peak shifts inversely towards lower diffraction angles, and the lattice constant slightly increases. It is possible that this behavior can be attributed to the incorporation of a part of the Si^{4+} ions into the interstitial sites of LuAG. Zhang *et al.*[10] also reported the same phenomenon for $Y_3Al_{5-x}Si_xO_{12-x}N_x$:$Ce^{3+}$ powders; they speculated that for $x \geq 0.3$, the Si^{4+} ions can occupy the interstitial sites, as well as the substitutional sites, of the YAG lattices, resulting in an expansion of the unit cell. An SEM micrograph of the powder prepared with x = 0.25 is shown in Fig. 1(c). The particle size is in the range of approximately 1 - 2.5 μm, while the particle morphology was nearly independent of the x values.

The PLE and PL spectra of the LuAG:0.035Ce^{3+} powders are shown in Fig. 3. The PLE spectrum is composed of two excitation bands, peaking at 345 nm and 450 nm, respectively; these spectra are assigned to the characteristic transition from the ground state (4f) doublet ($^2F_{7/2}$ and $^2F_{5/2}$) to the excitation levels (5d) of the Ce^{3+} ions. Under 450 nm

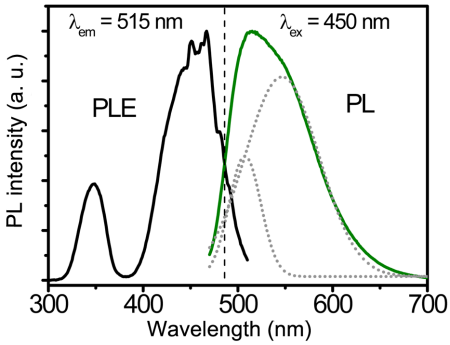

Fig. 3. PLE (λ_{em} = 515 nm) and PL spectra (λ_{ex} = 450 nm) of the LuAG:0.035Ce^{3+} powders. (Dotted lines represent the subbands of the 515 nm emission.)

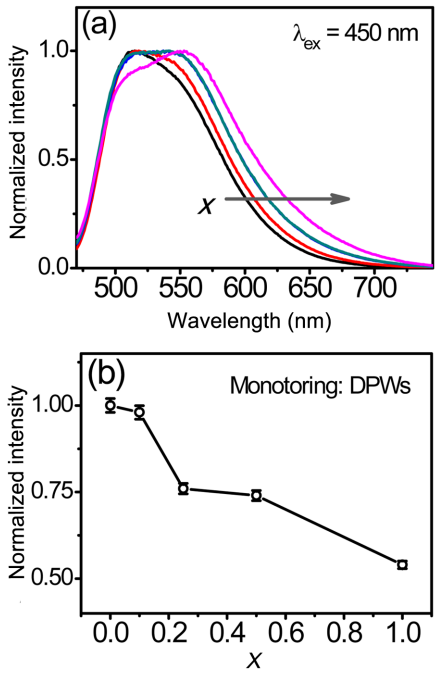

Fig. 4. (a) Normalized PL spectra and (b) emission intensity as a function of x of the (Lu,Ce)AG : xSN (x = 0–1.0) powders.

excitation, an asymmetrical emission spectrum was obtained in the green region (515 nm); this was the result of two overlapping subbands (dotted lines, centered at 507 and 546 nm, respectively), which can be assigned to the $^2D \rightarrow {}^2F_{5/2}$ and $^2D \rightarrow {}^2F_{7/2}$ transitions of the Ce^{3+} ions, respectively.[8,19,22)]

Normalized PL emission spectra of the (Lu,Ce)AG:xSN powders are shown in Fig. 4(a). With increasing x, the full width at half maximum (FWHM) of the band gradually increases from 96 to 122 nm, and the dominant peak wavelength (DPW) shifts from 515 to 555 nm (red-shift), leading to an increase in the Stokes shift from 2805 to 4204 cm^{-1}. Increasing x values led to a decrease in the emission intensity, as shown in Fig. 4(b). Corresponding CIE (Commission Internationale de l'Éclairage) chromaticity coordinates are shown in Fig. 5. These coordinates move from the green to

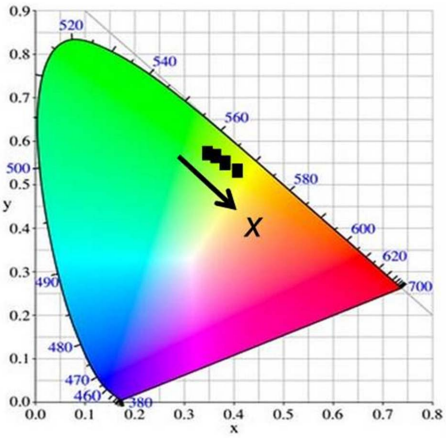

Fig. 5. CIE chromaticity coordinates of the (Lu,Ce)AG:xSN (x = 0–1.0) powders.

yellow regions with increasing x; they are (0.3493, 0.5727), (0.3658, 0.5658), (0.3847, 0.5512), (0.3847, 0.5496), and (0.4093, 0.5319) for x = 0, 0.1, 0.25, 0.5, and 1.0, respectively. It is inferred from these findings that the (Lu,Ce)AG:xSN powders have a potential for use in warm pc-WLEDs with high color rendering index (CRI).

It is obvious that the aforementioned spectral evolution of the (Lu,Ce)AG:xSN powders can be attributed to the incorporation of Si^{4+}–N^{3-} into the Al^{3+}–O^{2-} sites of LuAG. These behaviors can be explained based on those of YAG:Ce^{3+}, because the crystal structures of LuAG and YAG are nearly the same. For the $Y_3Al_{5-x}Si_xO_{12-x}N_x:Ce^{3+}$ powders, earlier works in the literature have described the effects of the incorporation of Si^{4+}–N^{3-} into the YAG:Ce^{3+} lattices differently. For example, some studies[10,12)] have reported that nitrogen was not detected in the synthesized powders, despite the addition of Si_3N_4. As a result, negative defects of V_{Al}''' were created to compensate for the three positive defects of $Si_{Al}^{\bullet}$, leading to a blue-shift of the DPWs, which is attributable to a change in the crystal field surroundings of the Ce^{3+} ions. On the other hand, other studies[9,11,13)] have confirmed the presence of Si^{4+}–N^{3-} bonds, which were found to cause a red-shift of the DPWs.

To verify the origin of the asymmetrical broadening and the red-shift of the emission band of the (Lu,Ce)AG:xSN powders, the emission spectrum (λ_{ex} = 450 nm) of the powders prepared with x = 1.0 was fitted using the Gaussian peak function, as shown in Fig. 6(a). The spectrum was split into three bands of (I), (II), and (III) centered at approximately 501, 545, and 597 nm, respectively. The sum of the fits coincides with the observed spectrum, indicating that this Gaussian fit is reasonable for the emission spectrum. Bands (I) and (II) correspond to two subbands of the emission spectrum of the LuAG:Ce^{3+} powders prepared without Si_3N_4 (Fig. 3), revealing that the addition of Si_3N_4 did not affect the two emission bands of LuAG:Ce^{3+}. On the other hand, the band (III) appears only for the (Lu,Ce)AG:xSN powders. It was inferred from this finding that additional

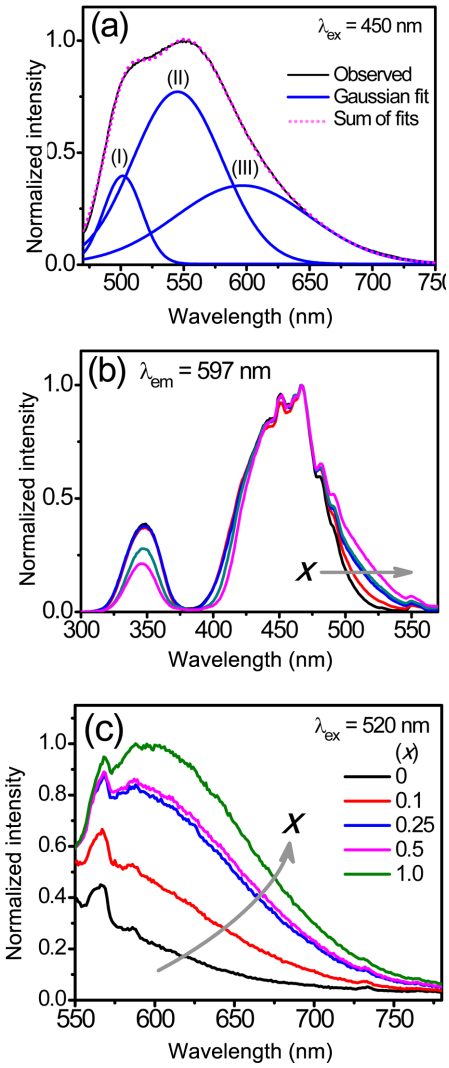

Fig. 6. (a) Gaussian fit for the PL spectrum (λ_{ex} = 450 nm) of the (Lu,Ce)AG:*x*SN powder prepared with x = 1.0. (b) Normalized PLE spectra (λ_{em} = 597 nm) and (c) PL spectra (λ_{ex} = 520 nm) of the (Lu,Ce)AG:*x*SN (x = 0–1.0) powders.

energy levels were created owing to the incorporation of Si^{4+}–N^{3-}. The PLE spectra for the band (III) (597 nm) were measured to determine the origin of the band (III). As a result, in addition to the characteristic excitation peaks at approximately 347 and 450 nm of LuAG:Ce^{3+}, low energy tails were observed in the range of 500–550 nm, and their intensities were found to increase with increasing x values, as shown in Fig. 6(b). The synthesized powders were activated by the wavelength of 520 nm belonging to the low energy tails; the PL spectra are shown in Fig. 6(c). The position and shape of the PL spectra for x = 0.25–1.0 evidently correspond to those of the band (III) in Fig. 6(a). For x = 0.1, the emission intensity at 597 nm rapidly drops; it is not observed for the LuAG:Ce^{3+} powders (x = 0). It was obvious from these findings that the band (III) and the low energy tail of the PLE spectrum were correlated with each other, and that they can be attributed to the incorporation of Si^{4+}–N^{3-} into the Al^{3+}–O^{2-} sites. The fact that the intensity of the low energy tail increases with increasing x values is a crucial piece of evidence for this speculation. These behaviors coincided with those in the earlier studies for $Y_3Al_{5-x}Si_xO_{12-x}N_x$:$Ce^{3+}$ [9,11,13] and (Lu,Ce)AG:*x*SN.[9,16] The addition of Si_3N_4 led to the local substitution of nitrogen ions for oxygen ions, which created two kinds of crystal field surroundings of the Ce^{3+} ions, Ce–O8 and Ce–(O,N)8 bonds. The latter have higher covalency and polarizability than the former, and the electronegativity of N^{3-} (~ 3.0) is lower than that of O^{2-} (~ 3.4). As a result, the Ce–(O,N)8 bonds enhanced the crystal field strength and lowered the centroid energy of the $5d^1$ split levels of the Ce^{3+} ions. The Ce–O8 bonds gave rise to the characteristic PLE and PL spectra of LuAG:Ce^{3+}. On the other hand, the Ce–(O,N)8 bonds caused extra $5d^1$ split levels of the Ce^{3+} ions, whose lowest excited level is closer to the ground state than is the lowest excited level of the Ce–O8 bond. This, in turn, resulted in low energy tails of the PLE spectra and the band (III) in the red region. In addition to the effects of local nitridation, it was probable that the substitution of the Si^{4+} ions for the Al^{3+} ions also contributed to the red-shift of the DPWs. The incorporation of smaller Si^{4+} ions distorted the cubic structure of LuAG and increased the degree of the crystal asymmetry, leading to an increase in the crystal field splitting.

Previous works have reported that the thermal stability of LuAG:Ce^{3+} was very high,[16,19] being comparable to nitride phosphors.[2,4,5] Liu *et al.* reported that the incorporation of Si^{4+}–N^{3-} rarely affected the thermal stability up to 150°C, irrespective of the x values.[19]

4. Conclusions

(Lu,Ce)AG:*x*SN powders were prepared with the addition of Si_3N_4 to LuAG:Ce^{3+}. XRD data confirmed that Si^{4+}–N^{3-} was fully incorporated into the LuAG lattices for x = 0–0.25, resulting in a decrease in the lattice constant because the Si^{4+} ions were smaller than the Al^{3+} ions. However, for x > 0.25, the lattice constant slightly increased because of the incorporation of a part of the Si^{4+} ions into the interstitial sites of LuAG.

The incorporation of Si^{4+}–N^{3-} into the Al^{3+}–O^{2-} sites of (Lu,Ce)AG:*x*SN resulted in a red-shift of the DPWs and low energy tails of the PLE spectra, leading to a migration of the CIE chromaticity coordinates from the green to yellow regions. These behaviors were attributed to the Ce–(O,N)8 bonds, which modified the $5d^1$ split levels and crystal field surroundings of the Ce^{3+} ions. These findings demonstrate that the (Lu,Ce)AG:*x*SN powders have potential for use in warm pc-WLEDs with high CRI.

Acknowledgements

This work was supported by Kyonggi University Research Grant 2014.

REFERENCES

1. J. McKittrick, M. E. Hannah, A. Piquette, J. K. Han, J. I. Choi, M. Anc, M. Galvez, H. Lugauer, J. B. Talbot, and K. C. Mishra, "Phosphor Selection Considerations for Near-UV LED Solid State Lighting," *ECS J. Solid State Sci. Technol*., **2** [2] R3119-31 (2013).
2. R.-J. Xie, N. Hirosaki, and T. Takeda, "Highly Reliable White LEDs Using Nitride Phosphors," *J. Korean Ceram. Soc*., **49** [4] 375-79 (2012).
3. W. Ahn, J. H. Park, and Y. J. Kim, "Synthesis, Phase Formation and Luminescence of $(Sr,Ba)_3MgSi_2O_8:Eu^{2+}$ by a Sol-Gel-Combustion Hybrid Process," *Ceram. Inter*., **41** S744-49 (2015).
4. J. Park, C. K. Lee, and Y. J. Kim, "Crystal Structure and Variation of Luminescence Properties of $(Ba,Ca)Si_7N_{10}:Eu^{2+}$ as a Function of the Eu and Ca Concentration," *Opt. Mater. Express*, **4** [6] 1257-66 (2014).
5. J. Park, S. J. Lee, and Y. J. Kim, "Evolution of Luminescence of $Sr_{2-y-z}Ca_zSi(O_{1-x}N_x):yEu^{2+}$ with N^{3-}, Eu^{2+} and Ca^{2+} Substitutions," *Cryst. Growth Des*., **13** [12] 5204-10 (2013).
6. Y. Narukawa, S. Saijou, Y. Kawakami, S. Fujita, T. Mukai, and S. Nakamura, "Radiative and Nonradiative Recombination Processes in Ultraviolet Light-Emitting Diode Composed of an $In_{0.02}Ga_{0.98}N$ Active Layer," *Appl. Phys. Lett*., **74** [4] 558-60 (1999).
7. E. Antic-Fidancev, J. Holsa, M. Lastusaari, and A. Lupei, "Dopant-Host Relationships in Rare-Earth Oxides and Garnets Doped with Trivalent Rare-Earth Ions," *Phys. Rev. B*, **64** 195108-1–195108-8 (2001).
8. D. J. Robbins, "The Effects of Crystal Field and Temperature on the Photoluminescence Excitation Efficiency of Ce^{3+} in YAG," *J. Electrochem. Soc*., **126** [9] 1550-55 (1979).
9. A. A. Setlur, W. J. Heward, M. E. Hannah, and U. Happek, "Incorporation of Si^{4+}-into Ce^{3+} - Doped Garnets for Warm White LED Phosphors," *Chem. Mat*., **20** [19] 6277-83 (2008).
10. F. Zhang, K. Song, J. Jian, S. Wu, P. Zheng, Q. Huang, J. Xu, and H. Qin, "Improvement of Photoluminescence Properties and Thermal Stability of $Y_{2.9}Ce_{0.1}Al_{5-x}O_{12}$ Phosphors with Si_3N_4 Addition," *J. Alloy. Compd*., **615** 588-93 (2014).
11. X. Wang, G. Zhou, H. Zhang, H. Li, Z. Zhang, Z. Sun, and J. Alloy, "Luminescent Properties of Yellowish Orange $Y_3Al_{5-x}Si_xO_{12-x}N_x$:Ce Phosphors and Their Applications in Warm White Light-Emitting Diodes," *J. Alloy. Compd*., **519** 149-55 (2012).
12. Y. S. Lin, Y. H. Tseng, R. S. Liu, and J. C. C. Chan, "Luminescent Properties and Structure Investigation of $Y_3Al_5O_{12}$/Ce Phosphors with Si Addition," *J. Electrochem. Soc*., **154** [2] P16-9 (2007).
13. M. Sopicka-Lizer, D. Michalik, J. Plewa, T. Juestel, H. Winkler, and T. Pawlik, "The Effect of Al-O Substitution for Si-N on the Luminescence Properties of YAG:Ce Phosphor," *J. Eur. Ceram. Soc*., **32** [7] 1383-87 (2012).
14. H. Luo, J. Liu, X. Zheng, B. Xu, Y. Lu, L. Han, K. Ren, and X. Yu, "Synthesis and Luminescence Properties of Mg-Si Co-Doped $Tb_3Al_5O_{12}:Ce^{3+}$ Phosphors with Blue Excitation for White LEDs," *J. Am. Ceram. Soc*., **95** [11] 3582-87 (2012).
15. W. Ahn and Y. J. Kim, "Effects of Flux on the Synthesis and the Luminescence of $Lu_3Al_5O_{12}:Ce^{3+}$ Phosphors," *Sci. Adv. Mater*., **8** [4] 904-8 (2016).
16. J. Liu, X. Wang, T. Xuan, C. Wang, H. Li, and Z. Sun, "$Lu_3(Al,Si)_5(O,N)_{12}Ce^{3+}$ Phosphors with Broad Emission Band and High Thermal Stability for White LEDs," *J. Lumin*., **158** 322-27 (2015).
17. J. Barta, V. Cuba, M. Pospisil, V. Jary, and M. Nikl, "Radiation-Induced Preparation of Pure and Ce-Doped Lutetium Aluminium Garnet and its Luminescent Properties," *J. Mater. Chem*., **22** 16590-97 (2012).
18. A. Birkel, K. A. Denault, N. C. George, C. E. Doll, B. Hery, A. A. Mikhailovsky, C. S. Birkel, B.-C. Hong, and R. Seshadri, "Rapid Microwave Preparation of Highly Efficient Ce^{3+}-Substituted Garnet Phosphors for Solid State White Lighting," *Chem. Mat*., **24** [6] 1198-204 (2012).
19. R. Praveena, L. Shi, K. H. Jang, V. Venkatramu, C. K. Jayasankar, and H. J. Seo, "Sol-Gel Synthesis and Thermal Stability of Luminescence of $Lu_3Al_5O_{12}:Ce^{3+}$ Nano-Garnet," *J. Alloy. Compd*., **509** [3] 859-63 (2011).
20. A. A. Setlur and A. M. Srivastava, "On the Relationship between Emission Color and Ce^{3+} Concentration in Garnet Phosphors," *Opt. Mater*., **29** [12] 1647-52 (2007).
21. Y.-N. Xu and W. Y. Ching, "Electronic Structure of Yttrium Aluminum Garnet ($Y_3Al_5O_{12}$)," *Phys. Rev. B*, **59** 10530-35 (1999).
22. J. L. Wu, G. Gundiah, and A. K. Cheetham, "Structure-Property Correlations in Ce-doped Garnet Phosphors for Use in Solid State Lighting," *Chem. Phys. Lett*., **441** [4-6] 250-54 (2007).